The Role of Material Parameters and Mechanical Stresses on Magnetic and Magnetostrictive Hysteresis

P. A. Voltairas[†], D. I. Fotiadis[†] and C. V. Massalas[‡*]

†: *Dept. of Computer Science, University of Ioannina, Ioannina GR 451 10, Greece*

‡: *Dept. of Mathematics, Div. of Appl. Math. and Mechanics, University of Ioannina, Ioannina GR 451 10 Greece*

December 16, 1998

Abstract

The proposed micromagnetic model [1] is extended to account for shearing strains. We assume that the ferromagnetic material is a single cubic crystal, the magnetization reverses coherently and the strains are uniform. The equilibrium field equations are derived from the free energy functional. The role of the material parameters and the applied stresses (*inverse magnetostriction effect*) on the magnetization and magnetostriction curves is examined in detail.

PACS: 75.60.-d; 75.70.-i; 75.80.+q

Keywords: Micromagnetics; Magnetostriction; Hysteresis; Thin Films; Inverse Magnetostriction Effect

*Corresponding Author. Tel.: +30 651 41800; fax: +30 651 42215; e-mail: cmasalas@cs.uoi.gr

1 Introduction

Understanding micromagnetic processes in magnetic materials plays a crucial role for the design of new magnetic storage devices with improved characteristics. Among the phenomena that are present in ferromagnetic materials, magnetostriction is the one that has not been studied in extent, due to its complexity. Magnetostrictive materials are very attractive for the production of microelectromechanical systems (MEMS), such as microrobots, micromotors, etc. [2, 3]. The magnetomechanical problem, in general, is extremely complicated due to its non-linear character [4–6]. Recently, new mathematical methods have utilized to treat the large magnetostriction observed in a class of ferromagnetic materials [7–9]. Those theories are applied on large enough materials, where the division of the crystal into domains is preferable, and thus are not capable of describing accurately the underlying microstructure. Savage and Spano proposed a rotational model that includes shear stresses to explain the large magnetoelastic coupling observed in Metglas 26005SC [10]. A probabilistic model for magnetostrictive and magnetic hysteresis in Terfenol-D compounds has been proposed by Armstrong [11]. The critical stresses that eliminate hysteresis in magnetostrictive materials were determined by Cullen et al. [12] for coherent magnetization reversal. Curling nucleation modes in elastic infinite circular ferromagnetic cylinder were studied in [13].

The main purpose of this work is to discuss, through micromagnetic principles, the role of shearing strains, applied mechanical loads and material parameters on the magnetization and magnetostriction curves of magnetostrictive ultra-

thin films. Ultra thin films can be treated approximately as fine single domain particles [14]. In the literature [15,16] the effects of stress and magnetostriction on the magnetization are studied assuming additional terms in the magnetic anisotropy energy density. In order to examine the combined effects of stress and magnetostriction on the magnetization reversal, a simple Stoner-Wohlfarth (SW) rotational model is introduced. Though the formulation is quite general and can be applied to materials with positive or negative magnetostriction, the discussion is limited to the case of cubic crystals with negative magnetostriction and magnetocrystalline anisotropy, like Ni. The results obtained are compared with those based on other models as well as on experiments.

2 The Variational Principle

According to the micromagnetic approach to the magnetomechanical problem [4, 5], the state of the deformable ferromagnetic material is described by the magnetization vector $\boldsymbol{\mu}(\boldsymbol{x})$ per unit mass ($\mu_i\,\mu_i = \mu_s^2 = const.$) and by the displacement vector $\boldsymbol{u}(\boldsymbol{x})$. Stable equilibrium states correspond to minima of the Gibbs free energy functional

$$G = \int_V (\rho_o F - w_m - w_H)\, dV_o - \int_{V_o} \rho_o \boldsymbol{f} \cdot \boldsymbol{u}\, dV_o - \int_{S_o} \boldsymbol{T} \cdot \boldsymbol{u}\, dS_o, \qquad (1)$$

where: $F(\mu_i, \mu_{i,j}, e_{ij})$ is the local internal energy per unit mass, e_{ij} are the infinitesimal strains ($e_{ij}(\boldsymbol{x}) = (u_{i,j} + u_{j,i})/2$), w_m is the magnetostatic self-energy per unit volume, w_H is the Zeeman energy density due to applied field $\boldsymbol{H}^o$, ρ_o is the mass density in the undeformed configuration, $\boldsymbol{f}$ are the body forces and $\boldsymbol{T}$ are the surface tractions.

In the present study we assume that the ultra-thin magnetostrictive film extends infinitely in y and z directions. In its undeformed state the thin film has its principal axes along the coordinate axes. The problem geometry is shown in Fig. 1. The specimen is a single crystal of cubic symmetry with its easy directions oriented along the coordinate axes, in the undeformed state. The present analysis relies on infinitesimal uniform strains described by:

$$e_{ij} = \begin{pmatrix} -e_L & 0 & 0 \\ 0 & 0 & e_S \\ 0 & e_S & e_L \end{pmatrix}. \tag{2}$$

Due to the assumptions made the Gibbs free energy functional (1) takes the following form [4, 5],

$$\begin{aligned} \tilde{G} &= K_1 \frac{\sin^2 2\theta}{4} + B_1\, e_L \cos^2\theta + B_2\, e_S \sin 2\theta - \mu_o M_s\, H_z^\circ \cos\theta + \\ &\quad + (c_{11} - c_{12})\, e_L^2 + \frac{c_{44}}{2}\, e_S^2 - e_L\, T \cos^2\psi - e_S\, T \sin 2\psi, \end{aligned} \tag{3}$$

where: $\tilde{G} \equiv G/V_o$, K_1 is the magnetocrystalline anisotropy constant, B_1, B_2 are the magnetoelastic constants, c_{11}, c_{12}, c_{44} are the elastic constants, T is the uniform surface traction and μ_o is the magnetic permeability of vacuum. Introducing the following dimensionless quantities:

$$\begin{aligned} & g = \tilde{G}/\mu_o M_s^2, \quad m = M_z/M_s = \cos\theta, \quad \sigma = T/\mu_o M_s^2, \quad h = H_z^\circ/M_s, \\ & h_k = 2K_1/\mu_o M_s^2, \quad h_{mel} = B_1/\mu_o M_s^2, \quad h_{mes} = B_2/\mu_o M_s^2, \\ & h_{el} = (c_{11} - c_{12})/\mu_o M_s^2, \quad h_{es} = c_{44}/2\mu_o M_s^2, \\ & \sigma_L = \sigma \cos^2\psi, \quad \sigma_S = \sigma \sin 2\psi, \end{aligned} \tag{4}$$

the dimensionless Gibbs free energy is given by

$$g(m,\, e_L,\, e_S) = h_k \frac{m^2(1-m^2)}{2} + h_{mel}\, e_L\, m^2 + 2h_{mes}\, e_S\, m\sqrt{1-m^2} -$$

$$- h\, m + h_{el}\, e_L^2 + h_{es}\, e_S^2 - \sigma_L\, e_L - \sigma_S\, e_S. \tag{5}$$

The terms on the right hand side of (5) represent successively: the anisotropy energy, the magnetoelastic energy, the Zeeman energy, the elastic energy and the energy due to the uniform surface tractions. The reduced magnetoelastic constants h_{mel} and h_{mes} can be related to the saturation magnetostriction constants λ_{100} and λ_{111} as follows [17]:

$$\begin{aligned} h_{mel} &= -\frac{3}{2}\lambda_{100}\, h_{el} \\ h_{mes} &= -3\lambda_{111}\, h_{es}. \end{aligned} \tag{6}$$

Minimization of the Gibbs free energy (5) with respect to the magnetization m, under constant strains e_L, e_S results in the magnetic constitutive law for the material that is:

$$h = h_k m\,(1 - 2m^2) + 2h_{mel}\, e_L\, m + 2h_{mes}\, e_S\, \frac{1 - 2m^2}{\sqrt{1 - m^2}}, \tag{7}$$

where the first term on the right hand side of (7) is of a pure magnetic origin, while the rest are due to magnetoelastic effects. Similarly, minimization of (5) with respect to the strains e_L and e_S, under constant magnetization m, results in the following stress-strain constitutive laws:

$$e_L = e_L(\sigma, \psi, m) = \frac{\sigma_L}{2h_{el}} - \frac{h_{mel}}{2h_{el}}\, m^2 \tag{8}$$

$$e_S = e_S(\sigma, \psi, m) = \frac{\sigma_S}{2h_{es}} - \frac{h_{mes}}{h_{es}}\, m\sqrt{1 - m^2}. \tag{9}$$

As expected, apart from the first term on the right hand sides of eqs. (8) and (9) that represent the pure mechanical in origin strains, the second terms account

for the magnetostrictive strains. The stability conditions for the energy minima (7-9) are the usual ones:

$$h_{el} > 0 \tag{10}$$

$$h_{es} > 0 \tag{11}$$

$$h_{es}\,(1-m^2)\left(h_{el}\,\frac{\partial^2 g}{\partial m^2} - 2h_{mel}^2\,m^2\right) - 2h_{el}\,h_{mes}^2\,(1-2m^2) > 0. \tag{12}$$

The conditions (10) and (11) are the well known stability criteria for ensuring the positive character of the pure elastic quadratic energy form. Due to (12) it is easily verified that the initial saturation state ($m = +1$) along the field direction is a stable state only for

$$h_{mes}\,\sigma_S < 0, \tag{13}$$

and since we our analysis is limited to materials with negative magnetostriction ($h_{mes} > 0$, due to Eqs. (6) and (10)), the condition (13) is satisfied for $\pi/2 < \psi < \pi$ and $3\pi/2 < \psi < 2\pi$, since $\sigma > 0$. This is expected, since for materials with negative magnetostriction, the stress direction becomes a hard axis ($\lambda_{111}\,\sigma < 0$) and if it is oriented in a small angle from the applied field direction, the magnetization has to overcome an energy barrier in order to be aligned with the applied field. For Ni the reduce material constants are given in Table 1.

3 Magnetization and Magnetostriction Curves

We note that in the cases $\psi = 0, \pi/2, \pi$ the effect of material parameters (h_k, h_{mel}, h_{mel}) and applied stresses (σ) on coercivity h_c and remanence m_r can be determined analytically, while in any other case numerical treatment of

the problem is needed.

3.1 Case 1 ($\psi = 0,\ \pi$)

In this case $\sigma_S = 0$, $\sigma_L = \sigma$ and solving Eq. (7) for m results in at most three real roots and thus a single jump in the magnetization curve that determines coercivity. This jump corresponds to $\partial h/\partial m = 0$. Since the magnetization curve is stress dependent this jump may not exist (anhysteretic magnetization reversal), provided that the stresses are larger than a critical value (σ_c) determined by the condition $(\partial h/\partial m)_{m=0} = 0$:

$$\sigma_c = \frac{h_{el}}{h_{mel}} \left(\frac{2h_{mes}^2}{h_{es}} - h_k \right). \tag{14}$$

The coercivity corresponds to $h_c = h(m_c)$ with m_c the roots of $\partial h/\partial m = 0$. Thus, since

$$m_c = \frac{1}{\sqrt{6}} \frac{\sqrt{1 - \frac{\sigma}{\sigma_c}}}{\sqrt{1 - \frac{h_{mel}}{2\,\sigma_c}}}, \tag{15}$$

the coercivity in given by

$$h_c = -\frac{1}{3}\sqrt{\frac{2}{3}} \frac{h_{mel}\,\sigma_c}{h_{el}} \frac{\left(1 - \frac{\sigma}{\sigma_c}\right)^{3/2}}{\sqrt{1 - \frac{h_{mel}}{2\,\sigma_c}}} \tag{16}$$

and the remanence ($h(m_r) = 0$) by

$$m_r = \sqrt{3}\, m_c = \frac{1}{\sqrt{2}} \frac{\sqrt{1 - \frac{\sigma}{\sigma_c}}}{\sqrt{1 - \frac{h_{mel}}{2\,\sigma_c}}}. \tag{17}$$

Equation (16) is analogous to the one obtained in the previous work on the effect of longitudinal stresses and magnetostriction, on the magnetization reversal [1, 18]. From Eqs. (16) and (17) it is deduced that for $\sigma = 0$ the increment in the coercivity and the remanence, is of the order of 10^{-2} for magnetoelastic

constant as large as $h_{mel} = 4 \times 10^3$, with $h_{mes} = 0$. This fact is illustrated in Fig. 2, for the coercivity. Notice that due to (16) the coercivity for the case of Ni decreases with the applied stress and vanishes for $\sigma \geq \sigma_c$. There is a critical region of stresses ($\sigma \geq \sigma_R$), where the hysteresis loop is rectangular, with the coercivity identical to the nucleation field h_n. The nucleation field is defined as the field where the initial equilibrium saturation state along the field direction becomes neutral ($\delta^2 g = 0$). This is obtained after substituting Eqs. (8) and (9) into (5) and linearizing the latter around the equilibrium state $m = +1$, that is:

$$h_n = -h_k - \frac{h_{mel}^2}{h_{el}} + \frac{2h_{mes}^2}{h_{es}} + \frac{h_{mel}\,\sigma}{h_{el}}. \tag{18}$$

This linear dependence of h_n on σ is analogous to the problem studied in [1]. Then, the critical stress (σ_R) for rectangular hysteresis is determined from the condition $(\partial h/\partial m)_{m=+1} = 0$:

$$\sigma_R = 3\,h_{mel} - 5\,\sigma_c. \tag{19}$$

For the case of Ni, $\sigma_R < 0$, and since $\sigma \geq 0$ there are no stresses for square hysteresis loop. Longitudinal and shear magnetostrictive curves are plotted in Fig. 3a and Fig. 3b for varying magnetocrystalline anisotropy constant. It is evident that for the given material constants, the stability criteria (10-12) result in hysteretic magnetostrictive curves. The sharp transitions observed along the initial strain curves, in both Figs. 3a-b, at a critical field value, are due to the crudeness of the model. It is obvious that for small anisotropy only small applied magnetic fields are capable to produce the resultant length change (strain) in the material. This is analogous to the case $e_S = 0$, studied previously [18].

Efficient performance of actuator devices require small anisotropies to produce the strain in the material [20]. In Fig. 4a and Fig. 4b we plotted magnetostrictive curves for varying applied stress σ. It is obvious that longitudinal stresses, apart from shifting the longitudinal strains along the strain axis [23], result, also, in both $e_L(h)$ and $e_S(h)$ curves in the formation of a *"hard strain axis"*. Thus, it is confirmed that stresses serve as a way to change the magnetocrytsalline anisotropy of the material.

3.2 Case 2 ($\psi = \pi/2$)

In this case $\sigma_S = \sigma_L = 0$ and thus the applied stress has no effect on the magnetization and magnetostriction curves. This is expected, since we assumed that the material is infinite along the stress direction. The coercivity and remanence correspond to $h_c(\sigma = 0)$ and $m_r(\sigma = 0)$ in Eqs. (16) and (17), respectively. They can equivalently be rewritten as:

$$h_c = h_c^{rigid} \frac{\left(1 - \frac{2\,h_{mes}^2}{h_{cs}\,h_k}\right)^{3/2}}{\sqrt{1 - \frac{2\,h_{mes}^2}{h_{cs}\,h_k} + \frac{h_{mel}^2}{2\,h_k}}}, \qquad h_c^{rigid} = \frac{h_k}{3}\sqrt{\frac{2}{3}} \tag{20}$$

and

$$m_r = m_r^{rigid} \frac{\left(1 - \frac{2\,h_{mes}^2}{h_{cs}\,h_k}\right)^{3/2}}{\sqrt{1 - \frac{2\,h_{mes}^2}{h_{cs}\,h_k} + \frac{h_{mel}^2}{2\,h_k}}}, \qquad m_r^{rigid} = \sqrt{\frac{h_k}{2}}. \tag{21}$$

3.3 Case 3 ($\psi \neq 0,\ \pi,\ \pi/2$)

In this case the equation $h(m) = 0$ has at most four real roots, which can not be obtained analytically. Thus there are at most six jumps in the magnetization curve determined by the solutions of the equation:

$$\frac{\partial h}{\partial m} = 0. \tag{22}$$

The nucleation field h_n is identical to that of Eq. (18) after replacing σ by σ_L, and thus depends on the stress orientation $h_n = h_n(\sigma, \psi)$. Due to the symmetry of the problem $h_c(\psi) = h_c(\pi \pm \psi)$ and $m_r(\psi) = m_r(\pi \pm \psi)$. The numerical solutions of Eq. (22) are summarized in Fig. 5, where we plotted the coercivity as a function of stress orientation ψ (Fig. 5a), for varying σ, and as a function of stress σ (Fig. 5b), for varying ψ. We included in Fig. 5a and the unstable branch of solutions ($0 < \psi < \pi/2$) since for materials with positive magnetostriction ($h_{mel}, h_{mes} < 0$) these become stable ones. In the particular case of Ni, the coercivities in Figs. 5(a-b) are as high as $H_c = 3.5\, M_s \simeq 139\,\mathrm{kA/m}$ for applied stresses as high as $T = 1.25 \times 10^4 \mu_o M_s^2 \simeq 250\,\mathrm{MPa}$. The curves labeled $\psi = \pi$ and $\pi/2$ in Fig. 5b correspond to the analytical solutions (16) and (20), respectively. For $\psi \neq \pi$ a minimum is observed in the $h_c(\sigma)$ curves, for some applied stress. This stress dependence of coercivity has been observed in experiments on amorphous ribbons and wires [21] and on pearlitic steel [22]. We also plotted and the remanence as a function of stress orientation angle ψ, for varying σ in Fig. 6a and as a function of σ for varying ψ in Fig. 6b. The remanence in the stable stress orientation region ($\pi/2 < \psi < \pi$), is always a decreasing function of ψ and σ. Typical magnetization curves for some specific points of the $h_c(\psi, \sigma)$ surface (see Figs. 5a-b) are presented in Fig. 7. Notice that for the case of Ni, $h_n > 0$ and thus the hysteresis loop can never become rectangular ($h_n = h_c$). The field axis is normalized with respect to the anisotropy field. Magnetostriction curves for longitudinal strains are plotted in Fig. 8 for varying anisotropy constant, for stress ratio $\sigma_S/\sigma_L = 4/5$, with $\sigma = 5 \times 10^4$. Like

in Fig. 3, small anisotropy needs only small applied field to produce the resultant strain in the material. The difference with the Case 1 is that, by taking into account shearing strains and for $\sigma_S \neq 0$, the magnetostricive curves are more realistic, in comparison with experiments, and do not show the sharp transitions that are present for $\psi = 0, \pi/2, \pi$. Finally, in Fig. 9 we plotted magnetostrictive curves for longitudinal (Fig. 9a) and shearing (Fig. 9b) strains, for varying σ_S, with $\sigma_L = 6 \times 10^4$. The magnetostrictive curves are also realistic and the applied stresses seems to form a *"hard strain axis"*, as it is the case of Fig. 4. This type of dependence of the magnetostriction curves on applied stresses has been observed in related experiments [23, 24].

4 Conclusions

In the present study a simple SW rotational model is proposed for both ferromagnetic and magnetostrictive hysteresis. The model accounts for all types of relations between material parameters. It is confirmed that the change in the coercivity and remanence due to magnetostriction is a second order effect. The effect of anisotropy on the magnetostrictive hysteresis dictates the region of efficient performance of actuator devices. The effect of applied stresses seems to be analogous to that of magnetocrystalline anisotropy, forming *"easy"* or *"hard strain axis"*, for materials with positive or negative magnetostriction, respectively. Inclusion of shearing strains (with $\sigma_S \neq 0$), in the model, resulted in more realistic magnetostriction curves, in comparison to the case where only pure longitudinal strains are taken into account [18]. Though the present study

is limited only to single ferromagnetic crystals, the minima in $h_c(\sigma, \psi)$ curves for $\pi/2 \leq \psi \leq \pi$ and $3\pi/2 \leq \psi \leq 2\pi$ are in qualitative agreement with related experiments on amorphous ribbons and wires [21] and further examination is needed in order to make this agreement quantitative.

References

[1] P.A. Voltairas, D.I. Fotiadis and C.V. Massalas, (accepted, Int. J. Eng. Sci.)

[2] K.I. Arai, T. Honda, Robotica 14 (1996) 477.

[3] E. A. Lindgren et al., J. Appl. Phys. 83 (1998) 7282.

[4] W. F. Brown, Magnetoelastic Interactions, Tracts of Natural Philosophy, Vol. 9 (Springer, Berlin, 1966).

[5] A. C. Eringen and G. A. Maugin, Electrodynamics of Continua I-II, (Springer-Verlag, NY, 1990); G. A. Maugin, Continuum Mechanics of Electromagnetic Solids, (North-Holland, Amsterdam, 1988).

[6] F. C. Moon, Magnetosolid Mechanics (John-Wiley and Sons, NY, 1984).

[7] R. D. James and D. Kinderleher, Cont. Mech. and Therm. 2 (1990) 215; Phil. Mag. B 68 (1993) 237.

[8] A. DeSimone, J. Int. Mat. Syts. and Str. 5 (1994) 787; Script. Metal. Mater. 33 (1995) 1869.

[9] A. DeSimone, R.D. James, J. Appl. Phys. 81 (1997) 5706.

[10] H. T. Savage and M. L. Spano, J. Appl. Phys. 53 (1982) 8092.

[11] W. D. Armstrong, J. Appl. Phys. 81 (1997) 2321; J. Appl. Phys. 81 (1997) 3548.

[12] J. R. Cullen, K. B. Hathaway and A. E. Clark, J. Appl. Phys. 81 (1997) 5417.

[13] C. V. Massalas and P. A. Voltairas J. Magn. Magn. Mat. 135 (1994) 271.

[14] A. Arrott in A. Hernando (Ed.) Nanomagnetism, Kluwer Academic Publishers, Netherlands, 1993, p.663.

[15] W. F. Brown, Micromagnetics (John Wiley and Sons, NY, 1963), p. 125.

[16] A. Aharoni, Introduction to the Theory of Ferromagnetism (Oxford University Press, NY 1996), p. 87.

[17] See Ref. [15], page 125.

[18] P. A. Voltairas, D. I. Fotiadis and C. V. Massalas, Proceedings of the 5^{th} National Congress on Mechanics, Ioannina, Greece, August 1998, p. 863.

[19] Landolt-Bornstein, Magnetic properties II1, (Springer-Berlin, 1962).

[20] A. E. Clark in E. P. Wohlfarth, (Ed.), Ferromagnetic Materials, Vol. 1, North-Holland, 1980, p. 531.

[21] R. Grossinger, et al. J. Mag. Mag. Mat., Vol. 83 (1990) 351; J.P. Sinnecker et al., J. Mag. Mag. Mat., 133 (1994) 20; R. Sato Turtelli et al., J. Appl.

Phys., 78 (1995) 2590; A.M. Severino et al., J. Mag. Mag. Mat., 103 (1992) 117; P.T. Squire et al., J. Mag. Mag. Mat., 132 (1994) 10.

[22] J.N. Makar and B.K. Tanner, J. Mag. Mag. Mat., 184 (1998) 193.

[23] K. Prajapati et al, IEEE Trans. Mag., 29 (1993) 3514.

[24] A. E. Clark, M. L. Spano and H. T. Savage, IEEE Trans. Mag., 19 (1983) 1964; M. L. Spano, A. E. Clark and M. Wun-Fogle, IEEE Trans. Mag., 26 (1990) 1751; A. E. Clark, M. Wun-Fogle and J. B. Restroff, IEEE Trans. Mag., 29 (1993) 3511; J. B. Restroff, M. Wun-Fogle and A. E. Clark, J. Appl. Phys., 83 (1998) 7288.

Figure 1: Problem geometry.

Figure 2: Variation of h_c with h_{mel} ($-4 \leq h_k \leq -3.7$ with step 0.1, $h_{mes} = 0$).

Figure 3: Magnetostriction curves (a) $-e_L$ and (b) e_S, vs. h, with $\sigma = 0$ and varying h_k.

Figure 4: Magnetostriction curves (a) $-e_L$ and (b) e_S, vs. h, with varying σ.

Figure 5: (a) Coercivity h_c vs. ψ for $0 \leq \sigma \leq 1.2 \times 10^5$, with step 1.5×10^4. (b) Coercivity h_c vs. σ for $\pi/2 \leq \psi \leq 23\pi/32$ (dashed lines) and $3\pi/4 \leq \psi \leq \pi$ (full lines) with step $\pi/32$.

Figure 6: (a) Remanence m_r vs. ψ, for $0 \leq \sigma \leq 1.2 \times 10^5$ with step 1.5×10^4. (b) Remanece m_r vs. σ for $\pi/2 \leq \psi \leq \pi$ with step $\pi/16$ and for $\psi = 253\pi/256$.

Figure 7: Typical magnetization curves at different parts of the $h_c(\sigma, \psi)$ phase diagram (Figs. 5- 6). (i) $\sigma = 1.25 \times 10^5$, $\psi = \pi/2$, (ii) $\sigma = 1.25 \times 10^5$, $\psi = 9\pi/16$, (iii) $\sigma = 4.2 \times 10^3$, $\psi = 13\pi/16$, (vi) $\sigma = 5 \times 10^4$, $\psi = 15\pi/16$, (v) $\sigma = 1.25 \times 10^5$, $\psi = 15\pi/16$, (vi) $\sigma \geq \sigma_c$, $\psi = \pi$.

Figure 8: Magnetostriction curves $-e_L$ vs. h, with $\sigma_S/\sigma_L = 4/5$, $\sigma = 5 \times 10^4$ and for varying h_k.

Figure 9: Magnetostriction curves (a) $-e_L$ and (b) e_S, vs. h, with $\sigma_L = 6 \times 10^4$, $\sigma_S = 2\,\sigma_L \tan\psi$ and for varying ψ.

h_k	h_{mel}	h_{mes}	h_{el}	h_{es}
-4.28	3581	1749	47752208	58307959

Table 1: Dimensionless material constants for Ni [1, 19].

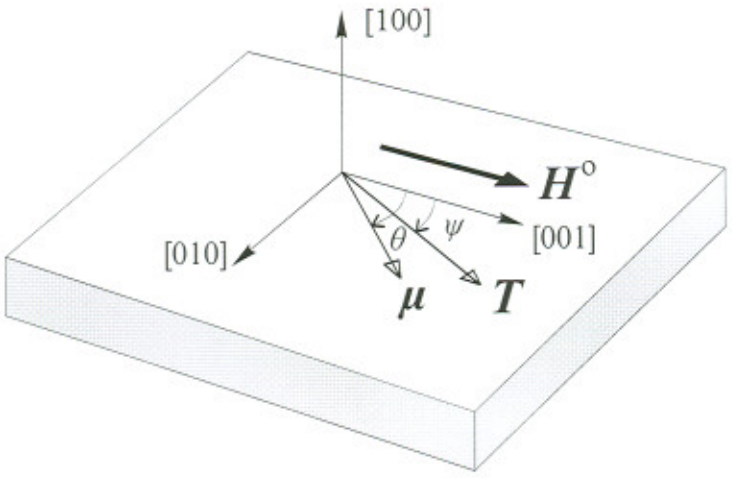

Fig. 1

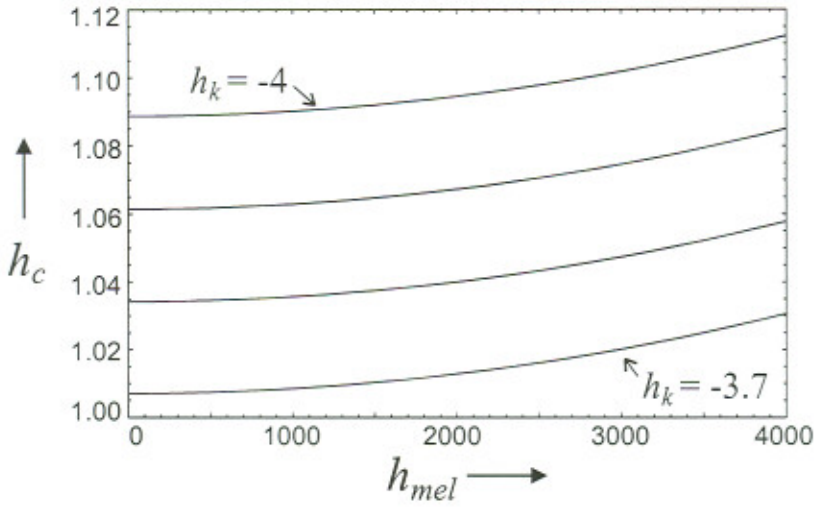
1.12
1.10
1.08
1.06
1.04
1.02
1.00
h_c
h_k = -4
h_k = -3.7
0
1000
2000
3000
4000
h_{mel}

Fig. 2

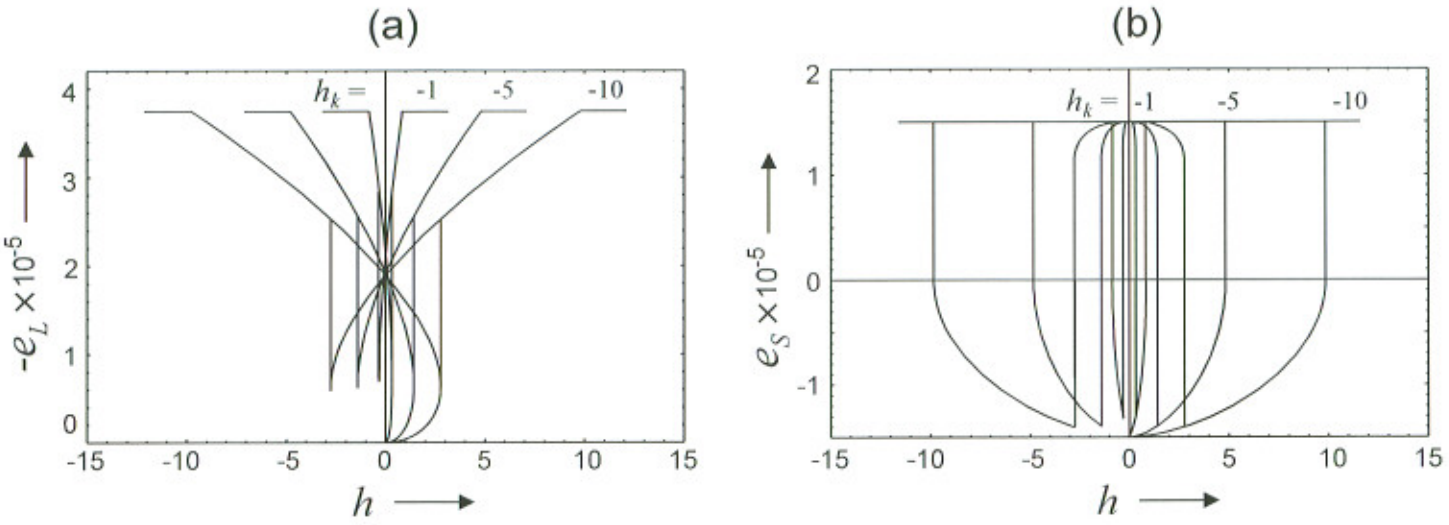

Fig. 3

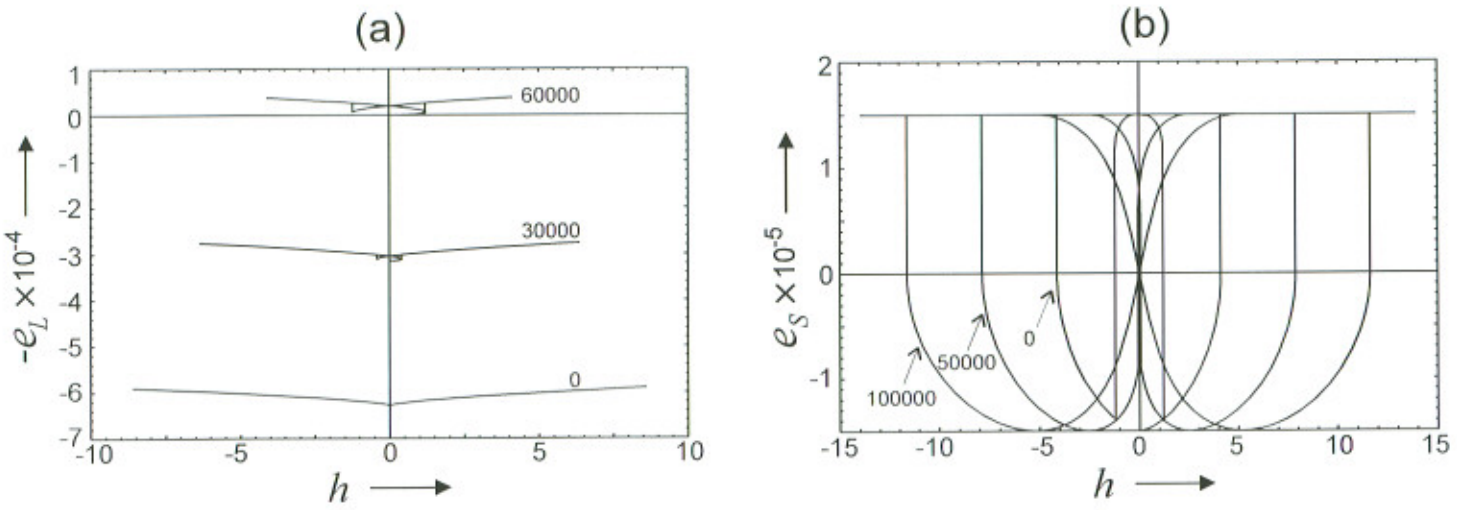

Fig. 4

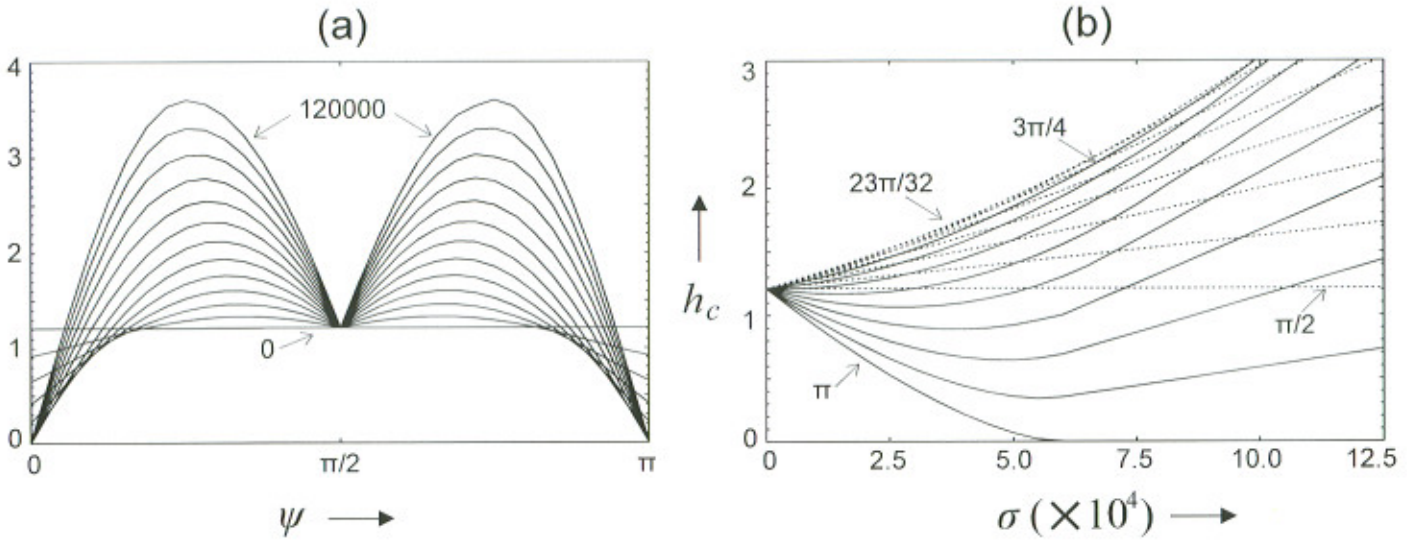
(a)
(b)
120000
0
3π/4
23π/32
π/2
π
h_c
ψ ⟶
σ ($\times 10^4$) ⟶
0
π/2
π
0
2.5
5.0
7.5
10.0
12.5

Fig. 5

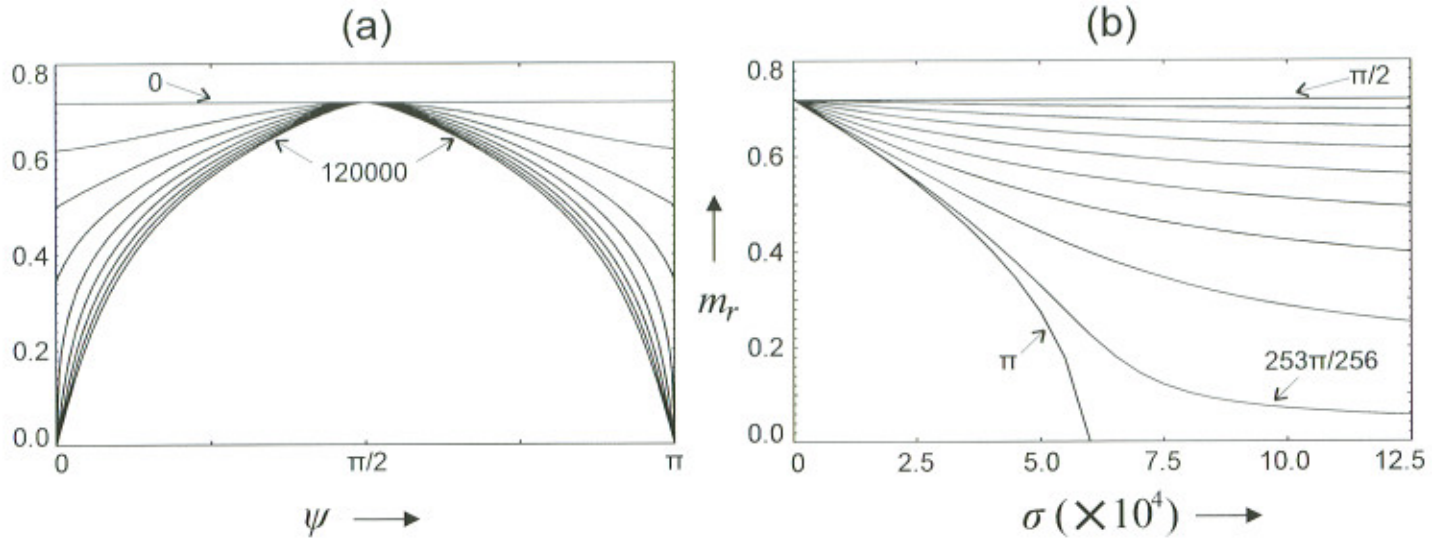
(a)
(b)
0.8
0.6
0.4
0.2
0.0
0
π/2
π
0
120000
ψ ⟶
m_r
π/2
π
253π/256
2.5
5.0
7.5
10.0
12.5
σ ($\times 10^4$) ⟶

Fig. 6

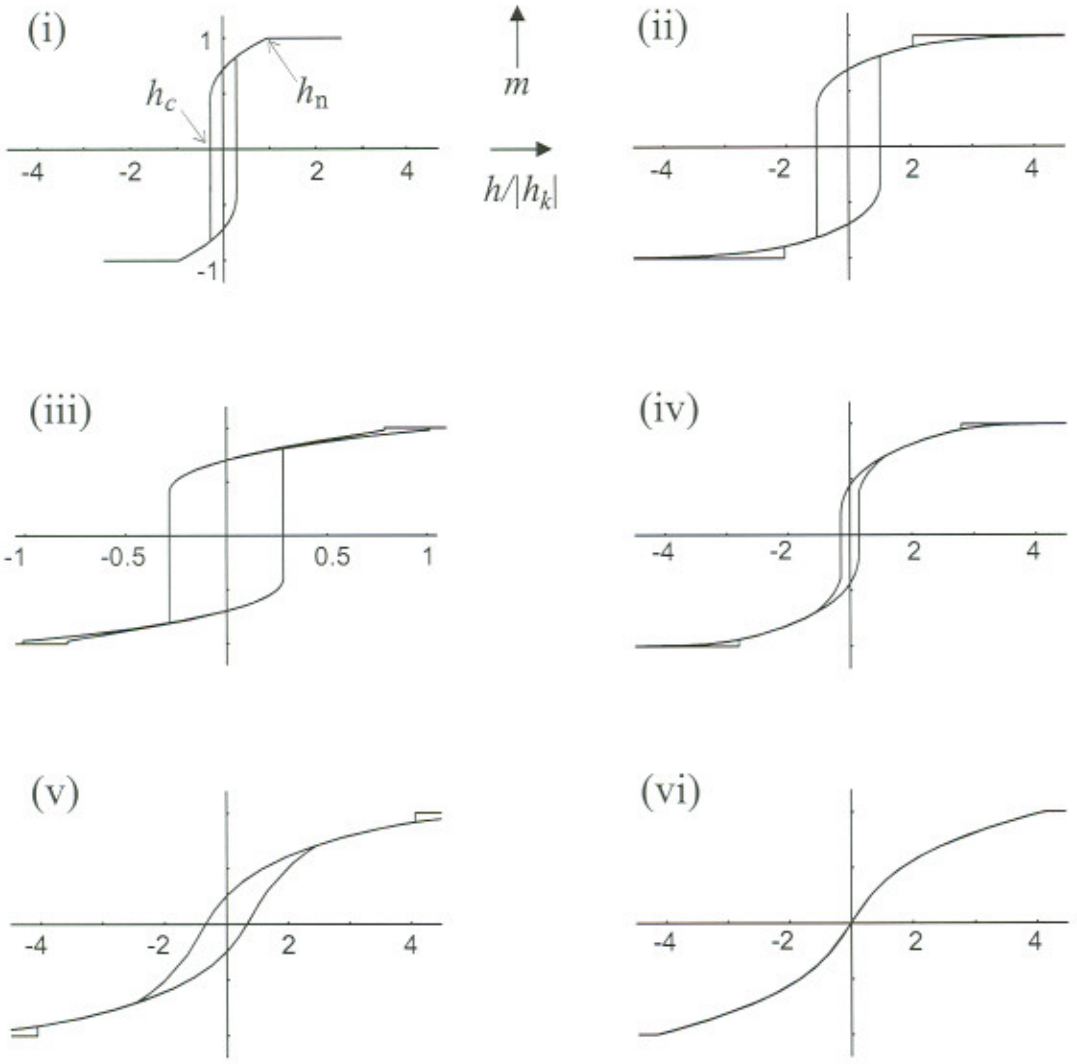

Fig. 7

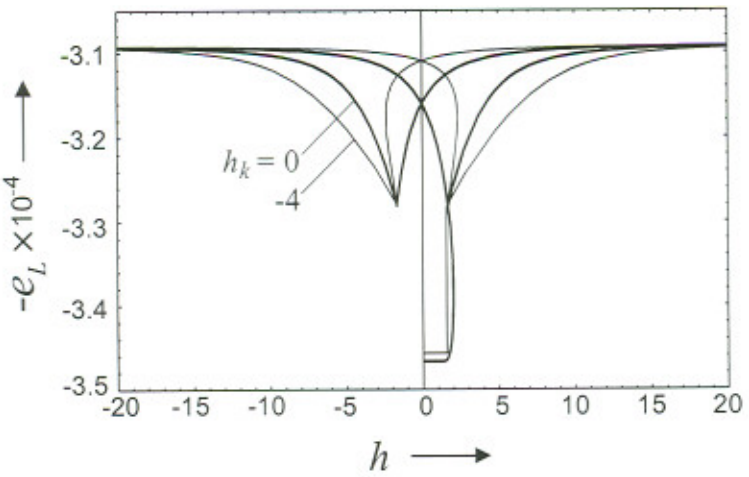

Fig. 8

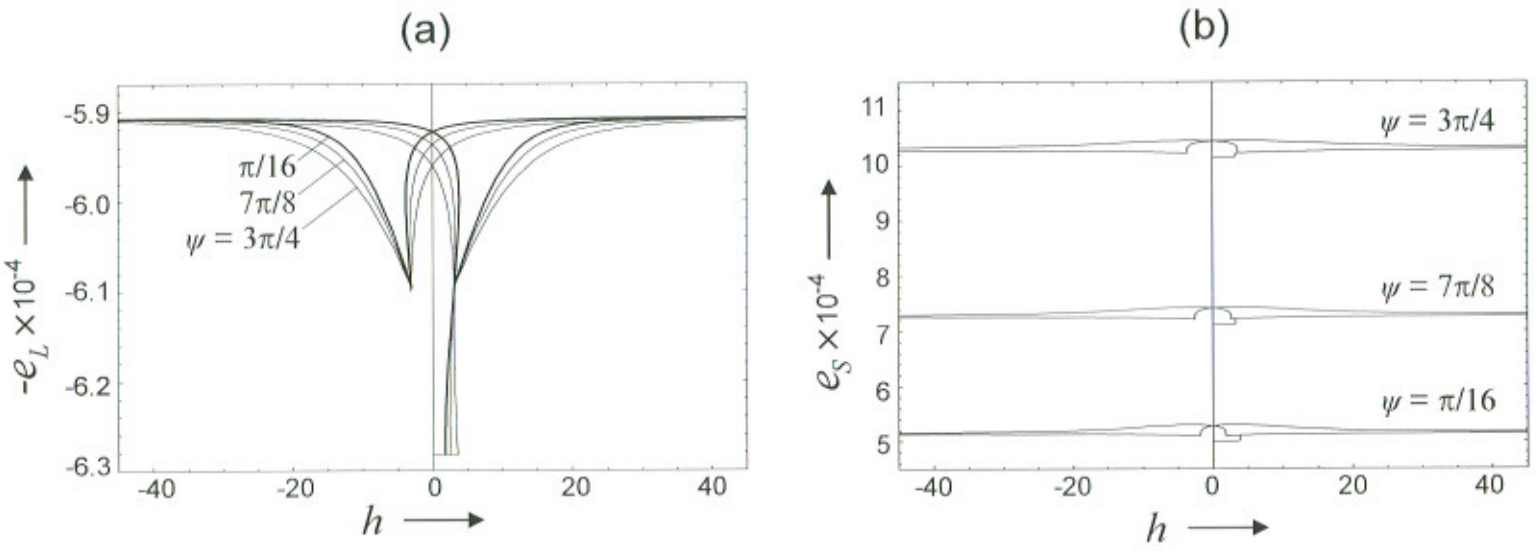
(a)
(b)
-5.9
-6.0
-6.1
-6.2
-6.3
-40
-20
0
20
40
h
$-e_L \times 10^{-4}$
π/16
7π/8
ψ = 3π/4
11
10
9
8
7
6
5
$e_S \times 10^{-4}$
ψ = 3π/4
ψ = 7π/8
ψ = π/16

Fig. 9